OPTICAL REVIEW Vol. 5, No. 5 (1998) 295-302

# Theoretical Treatment of Electric and Magnetic Multipole Radiation Near a Planar Dielectric Surface Based on Angular Spectrum Representation of Vector Field

Tetsuya INOUE and Hirokazu HORI

*Department of Electronics, Yamanashi University, 4-3-11, Takeda, Kofu, 400-8511 Japan*

(Received May 19, 1998; Accepted June 30, 1998)

We have developed an analytic treatment of light emission properties of electric and magnetic multipoles near a planar dielectric surface, using angular spectrum representation of vector spherical waves. The results are described in terms of spatial rotation matrix elements, so that the angular distribution of light emission for higher order multipoles is easily obtained, which enables us to evaluate basic optical near-field problems such as electric dipole radiation with arbitrary orientation with respect both to surface and observation direction. The numerical results are in good agreement with our previous experimental results and the numerical results reported by Lukosz.

**Key words:** optical near-field, evanescent wave, dielectric surface, multipole, angular spectrum

## 1. Introduction

Light emission characteristics near material surfaces have been extensively studied in relation to near field optics[1] and cavity quantum electrodynamics (cavity QED) problems.[2,3] On this subject, we have reported the experimental observation of light emission characteristics from excited atoms near a planar dielectric surface by means of laser spectroscopy using the Cs-$D_2$ line.[4] According to Snell's law, the homogeneous plane wave traveling from a dielectric medium with higher refractive index can be transmitted to a medium with lower refractive index only in directions within the critical angle of total internal reflection. This is not the case for light emission from an excited atom which is placed within subwavelength vicinity of the dielectric surface (optical near-field regime), because the light emitted by the excited atom includes both homogeneous and evanescent waves. The decay rate and angular distribution of radiation from an atomic dipole near a planar dielectric surface have been studied in detail, both experimentally and theoretically.[5-9] The experimental results are in good agreement with the results of the classical electromagnetic theory. Especially, Lukosz[9] derived analytic expressions for the angular distribution of light emission from classical electric and magnetic dipoles with arbitrary orientation, using a combination of one-component magnetic Hertz vector with one-component electric Hertz vector in order to solve the boundary value problem exactly.

In this paper, we studied the light scattering processes from electric and magnetic multipoles near a planar dielectric surface and derived analytic expressions for angular distribution of light emission, using angular spectrum representation of vector spherical waves which were reported briefly in our previous work.[10] As an example of application, we have compared numerical results with the experiment reported in our previous work.[4]

E-mail: hirohori@willow.esd.yamanashi.ac.jp

## 2. The Angular Spectrum Representation of the Vector Spherical Wave

We consider a space, half of which is filled with a non-magnetic, transparent, homogeneous, and isotropic medium of refractive index $n$ (the dielectric side $z<0$), and the other half a vacuum (the vacuum side $z\geq 0$) (see Fig. 1). Let us consider a classical point electric and magnetic multipole located in the vacuum at a position $\mathbf{R}$ directed from the origin on the $z=0$ plane. The radiation field from the classical electric and magnetic $2^J$-pole is characterized by wavenumber $K$, total angular momentum $J$, its $z$ projection $m$, and polarization state $\lambda$ (electric $\lambda=$E or magnetic $\lambda=$M).[11] Here, we consider a relative coordinate system $\mathbf{r}_0=\mathbf{r}-\mathbf{R}$ (see Fig. 1), in which the multipole is at its origin $z_0=0$ with $z_0$ axis being perpendicular to the dielectric surface. In the following discussion, we will refer to $z_0>0$ ($z_0<0$) space as the upper (lower) half-space of the multipole.

The vector potential radiated by the electric (E) and magnetic (M) $2^J$-poles is described, respectively, in terms of vector spherical wave[11] as follows:

$$\mathbf{A}^{\mathrm{E(RA)}}_{K,J,m}(\mathbf{r}_0)=i^{J+1}\sqrt{\frac{J}{2J+1}}h^{(1)}_{J+1}(\rho_0)\mathbf{Y}_{J,J+1,m}(\hat{\mathbf{r}}_0)+i^{J-1}\sqrt{\frac{J+1}{2J+1}}h^{(1)}_{J-1}(\rho_0)\mathbf{Y}_{J,J-1,m}(\hat{\mathbf{r}}_0)\,, \quad (1)$$

$$\mathbf{A}^{\mathrm{M(RA)}}_{K,J,m}(\mathbf{r}_0)=i^{J}h^{(1)}_{J}(\rho_0)\mathbf{Y}_{J,J,m}(\hat{\mathbf{r}}_0)\,, \quad (2)$$

where the unit vector $\hat{\mathbf{r}}_0=\mathbf{r}_0/r_0$, $\rho_0=Kr_0$, $h^{(1)}_l(\rho_0)$ the spherical Hankel function of the first kind, and $\mathbf{Y}_{J,l,m}(\hat{\mathbf{r}}_0)$ the vector spherical harmonics.[12] It is noted that the phase factors in Eqs. (1) and (2) are different from those appearing in popular textbooks such as Refs. 11, 12). Our definition is taken for convenience so that no additional phase factor remains in angular spectrum representations of vector spherical waves.

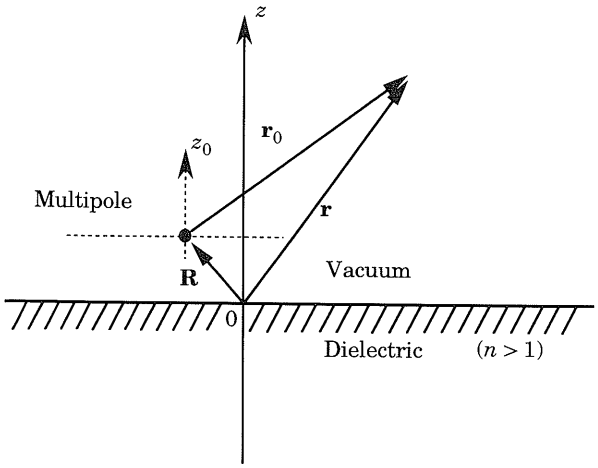


Fig. 1. Multipole plus planar dielectric surface system considered in this paper. The upper half-space ($z>0$) is a vacuum and the lower half-space ($z<0$) is filled with an isotropic medium of refractive index $n$. A classical point electric and magnetic multipole is located at $\boldsymbol{R}=(x_R,y_R,z_R)$. An Auxiliary coordinate system relative to the point multipole is also indicated.

In order to solve the planar boundary value problem, it is convenient to expand the vector multipole field into vector plane waves by means of angular spectrum representation.[10] The state of vector plane waves propagating in an arbitrary direction is characterized by wavenumber $K$, directional angle of wavevector $(\alpha,\beta)$, and polarization state $\mu$ (transverse electric wave, $\mu$=TE, or transverse magnetic wave, $\mu$=TM) with respect to the wavevector (see Fig. 2). The vector plane waves are described in the form of

$$\hat{\mathbf{s}}_\mu e^{iK\hat{\mathbf{s}}\cdot\mathbf{r}_0} \qquad (\mu=\mathrm{TE},\mathrm{TM}), \tag{3}$$

where the directional unit vector $\hat{\mathbf{s}}$ and polarization vectors $\hat{\mathbf{s}}_{\mathrm{TM}}$, $\hat{\mathbf{s}}_{\mathrm{TE}}$ with spherical polar angles $(\alpha,\beta)$ are defined, respectively, as

$$\begin{aligned}\hat{\mathbf{s}}&=\hat{\mathbf{s}}(\alpha,\beta)=(\sin\alpha\cos\beta,\ \sin\alpha\sin\beta,\ \cos\alpha),\\ \hat{\mathbf{s}}_{\mathrm{TM}}&=\hat{\mathbf{s}}_{\mathrm{TM}}(\alpha,\beta)=(\cos\alpha\cos\beta,\ \cos\alpha\sin\beta,\ -\sin\alpha),\\ \hat{\mathbf{s}}_{\mathrm{TE}}&=\hat{\mathbf{s}}_{\mathrm{TE}}(\alpha,\beta)=(-\sin\beta,\ \cos\beta,\ 0).\end{aligned} \tag{4}$$

Then, vector spherical waves are expanded into the vector plane wave as

$$\mathbf{A}^{(\mathrm{RA})}_{K,J,m}(\boldsymbol{r}_0)=\frac{1}{2\pi}\sum_{\mu}^{\mathrm{TE,TM}}\int_{C_\pm}\int_{-\pi}^{+\pi}d\Omega_{\hat{\mathbf{s}}}(\mu,\alpha,\beta|\lambda,J,m)\hat{\mathbf{s}}_\mu e^{iK\hat{\mathbf{s}}\cdot\mathbf{r}_0}, \tag{5}$$

where $d\Omega_{\hat{\mathbf{s}}}=\sin\alpha d\alpha d\beta$.[10] This corresponds to the angular spectrum representation of multipole field. The angle $\beta$ $(-\pi\le\beta<+\pi)$ is real, and $\alpha$ takes the complex contour $C_\pm$, ($C_+$ when $z_0>0$, and $C_-$ when $z_0<0$) as indicated in Fig. 3. This shows that the multipole field is composed of both homogeneous and evanescent waves. In this representation, the expansion coefficient $(\mu,\ \alpha,\ \beta|\lambda,\ J,\ m)$ corresponds to the analytically continued rotation matrix elements with respect to the angle $\alpha$. The particular form of these coefficients is given by[10]

$$(\mathrm{TE},\ \alpha,\ \beta|\mathrm{M},\ J,\ m)=\sqrt{\frac{2J+1}{8\pi}}\left(+\frac{i}{\sqrt{2}}\right)[D^{(J)*}_{m,+1}(\hat{\mathbf{s}})-D^{(J)*}_{m,-1}(\hat{\mathbf{s}})] \tag{6}$$

$$(\mathrm{TE},\ \alpha,\ \beta|\mathrm{E},\ J,\ m)=\sqrt{\frac{2J+1}{8\pi}}\left(-\frac{i}{\sqrt{2}}\right)[D^{(J)*}_{m,+1}(\hat{\mathbf{s}})+D^{(J)*}_{m,-1}(\hat{\mathbf{s}})], \tag{7}$$

where $D^{(J)}_{m,m'}(\hat{\mathbf{s}})=\langle J,m|e^{-iJ_z\beta}e^{-iJ_y\alpha}|J,m'\rangle$ are the rotation matrix elements. The others are obtained using the following relation:

$$(\mu,\ \alpha,\ \beta|\lambda,\ J,\ m)=i\eta_\mu(\bar{\mu},\ \alpha,\ \beta|\bar{\lambda},\ J,\ m). \tag{8}$$

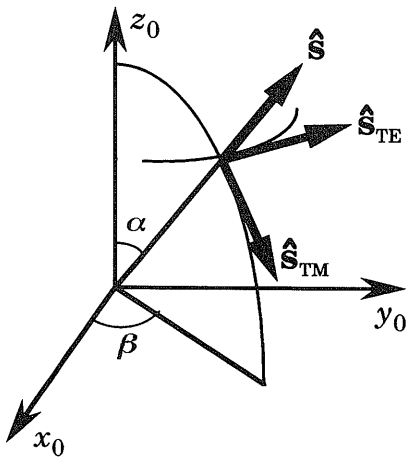


Fig. 2. Geometrical relation of wavevector and polarization vectors. $\hat{\mathbf{s}}$ is a unit wavevector, $\hat{\mathbf{s}}_{\mathrm{TE}}$, $\hat{\mathbf{s}}_{\mathrm{TM}}$ transverse electric (TE) and transverse magnetic (TM) polarization vectors. $\hat{\mathbf{s}}$, $\hat{\mathbf{s}}_{\mathrm{TM}}$, $\hat{\mathbf{s}}_{\mathrm{TE}}$ form the three orthogonal unit vectors in the spherical coordinate.

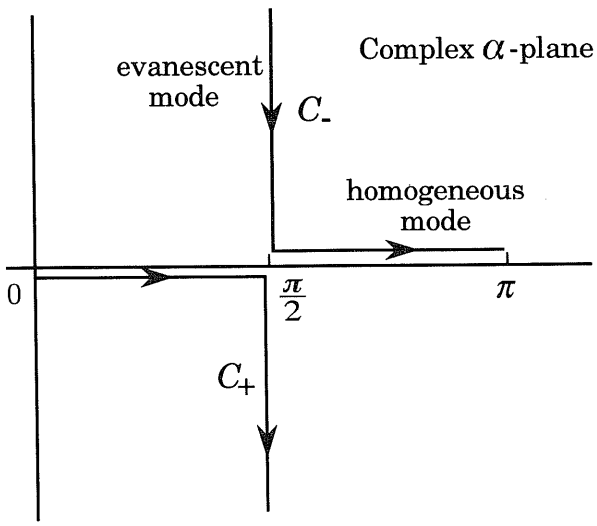


Fig. 3. The contour $C$ of integration for the rotation angle $\alpha$.
● The contour $C_+$ corresponds to the scattered wave in $z>0$ half-space. [$0\le Re[\alpha]<\pi/2$, $Im[\alpha]=0$; *homogeneous mode*], [$Re[\alpha]=\pi/2$, $0\ge Im[\alpha]>-\infty$; *evanescent mode*].
● The contour $C_-$ corresponds to the scattered wave in $z<0$ half-space. [$Re[\alpha]=\pi/2$, $\infty>Im[\alpha]\ge 0$; *evanescent mode*]. [$\pi/2<Re[\alpha]\le\pi$, $Im[\alpha]=0$; *homogeneous mode*].

Here, $\bar{\mu}$ and $\bar{\lambda}$ stand for the interchange of suffices $\mu$ and $\lambda$, respectively, and $\eta_{\mathrm{TM}}=+1$ and $\eta_{\mathrm{TE}}=-1$. As discussed previously,[10] one of the advantages of using rotation matrix elements is that the polarization characteristics of evanescent waves are directly derived from that of propagating plane waves with well defined states of polarization. Furthermore, a unified formulation can be obtained for transforms between the plane, cylindrical, and spherical vector mode functions as the basis of near-field optics, which was also studied earlier.[10]

Using $s_x=\sin\alpha\cos\beta$ and $s_y=\sin\alpha\sin\beta$, the angular spectrum representation, Eq. (5), is rewritten in the following alternative form[13]:

$$\mathbf{A}^{\lambda(\mathrm{RA})}_{K,J,m}(\mathbf{r}_0)=\frac{\pm 1}{2\pi}\sum_{\mu}^{\mathrm{TE,TM}}\int_{-\infty}^{+\infty}\int_{-\infty}^{+\infty}\frac{ds_x ds_y}{s_z}(\mu,\alpha,\beta|\lambda,J,m)\hat{\mathbf{s}}_\mu e^{iK\hat{\mathbf{s}}\cdot\mathbf{r}_0}, \tag{9}$$

where

$$\begin{aligned} s_z=\cos\alpha&=\pm\sqrt{1-\sin^2\alpha}\quad(\sin^2\alpha\le 1)\\ &=\pm i\sqrt{\sin^2\alpha-1}\quad(\sin^2\alpha>1)\end{aligned} \tag{10}$$

In Eqs. (9) and (10), the sign (+) is for $z_0>0$, and (−) for $z_0<0$. The angular spectrum representation of the form of Eq. (9) is frequently used in the calculation of scattered light in far-field optics. The asymptotic form of this representation has been investigated in several reports.[14–16]

## 3. Reflected and Transmitted Multipole Fields by Planar Dielectric Surface

In this section, we study the reflected and transmitted multipole field by the planar dielectric surface. Using the angular spectrum representation in the form of Eq. (5), the evaluation of the planar boundary value problem is straightforward. Let us consider the field emitted by the multipole into its lower half-space $z_0<0$ of the multipole, which corresponds to the incident field on the dielectric surface. We label this component by superscript I; the reflected and transmitted components are labeled by superscripts R and T, respectively (see Fig. 4). The vector potential is expressed by the integral corresponding to the contour $C_-$ in Eq. (5). We can rewrite Eq. (5) as

$$\begin{aligned}\mathbf{A}^{\lambda(\mathrm{I})}_{K,J,m}(\mathbf{r})&=\frac{1}{2\pi}\sum_{\mu}\int_{C_-}\int_{-\pi}^{+\pi}d\Omega_{\hat{\mathbf{s}}}f_{\lambda,J,m}(\mu,\alpha,\beta)\hat{\mathbf{s}}^{(\mathrm{I})}_\mu e^{iK\hat{\mathbf{s}}^{(\mathrm{I})}\cdot r},\\ &\quad\text{for } 0\le z<z_{\mathrm{R}}\ (\text{or } -z_{\mathrm{R}}\le z_0<0),\end{aligned} \tag{11}$$

where $\mathbf{r}_0=\mathbf{r}-\mathbf{R}$, $\mathbf{r}=(x,y,z)$, $\mathbf{R}=(x_{\mathrm{R}},y_{\mathrm{R}},z_{\mathrm{R}})$, and $\hat{\mathbf{s}}^{(\mathrm{I})}$ and $\hat{\mathbf{s}}^{(\mathrm{I})}_\mu$ indicate $\hat{\mathbf{s}}(\alpha,\beta)$ and $\hat{\mathbf{s}}_\mu(\alpha,\beta)$, respectively. The expansion coefficients are defined by

$$f_{\lambda,J,m}(\mu,\alpha,\beta)=(\mu,\alpha,\beta|\lambda,J,m)e^{-iK\hat{\mathbf{s}}(\alpha,\beta)\cdot\mathbf{R}}, \tag{12}$$

The incident electric multipole field onto the dielectric surface is obtained by using the following relation between the electric field and the vector potential,

$$\mathbf{E}(\mathbf{r},t)=-(\partial/\partial t)\mathbf{A}(\mathbf{r},t)=iK\mathbf{A}(\mathbf{r},t), \tag{13}$$

where the coefficient $iK$ arises due to temporal differentiation of the assumed monochromatic radiation field, $e^{-iKt}$. The electric multipole fields corresponding to the incident,

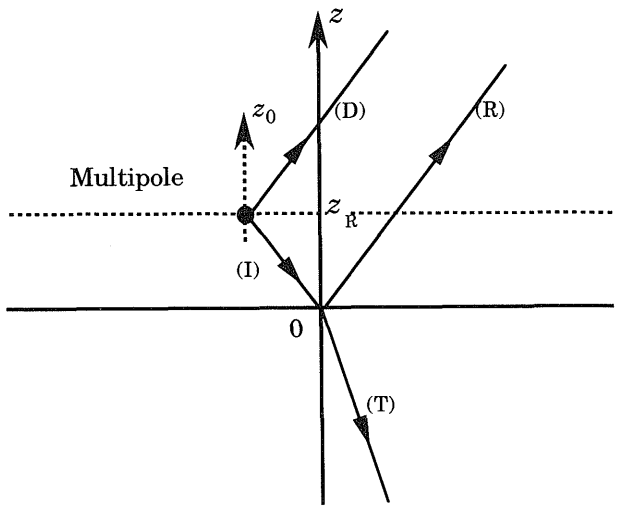


Fig. 4. The field components considered in the multipole plus dielectric surface system: (D) directly emitted field from multipole, (I) incident multipole field on the dielectric surface, (R) reflected multipole field, (T) transmitted multipole field. The field is described by (D) plus (R) for $z_{\mathrm{R}}<z$, and by (I) plus (R) for $0\le z<z_{\mathrm{R}}$, and by (T) for $z<0$.

reflected, and transmitted waves are written respectively by

$$\begin{aligned}\mathbf{E}^{\lambda(\mathrm{I})}_{K,J,m}(\mathbf{r})&=\frac{iK}{2\pi}\sum_{\mu}\int_{C_-}\int_{-\pi}^{+\pi}d\Omega_{\hat{\mathbf{s}}}f_{\lambda,J,m}(\mu,\alpha,\beta)\hat{\mathbf{s}}^{(\mathrm{I})}_\mu e^{iK\hat{\mathbf{s}}^{(\mathrm{I})}\cdot r},\\ &\quad\text{for } 0\le z<z_{\mathrm{R}}\ (z_0<0),\\ &=0,\ \text{for } z<0,\ z_{\mathrm{R}}<z\end{aligned} \tag{14}$$

$$\begin{aligned}\mathbf{E}^{\lambda(\mathrm{R})}_{K,J,m}(\mathbf{r})&=\frac{iK}{2\pi}\sum_{\mu}\int_{C_-}\int_{-\pi}^{+\pi}d\Omega_{\hat{\mathbf{s}}}f_{\lambda,J,m}(\mu,\alpha,\beta)\Re_\mu\hat{\mathbf{s}}^{(\mathrm{R})}_\mu e^{iK\hat{\mathbf{s}}^{(\mathrm{R})}\cdot r},\\ &\quad\text{for } z\ge 0\\ &=0,\ \text{for } 0<z\end{aligned} \tag{15}$$

$$\begin{aligned}\mathbf{E}^{\lambda(\mathrm{T})}_{K,J,m}(\mathbf{r})&=\frac{iK}{2\pi}\sum_{\mu}\int_{C_-}\int_{-\pi}^{+\pi}d\Omega_{\hat{\mathbf{s}}}f_{\lambda,J,m}(\mu,\alpha,\beta)\mathfrak{T}_\mu\hat{\mathbf{s}}^{(\mathrm{T})}_\mu e^{inK\hat{\mathbf{s}}^{(\mathrm{T})}\cdot r},\\ &\quad\text{for } z<0\\ &=0,\ \text{for } z\ge 0\end{aligned} \tag{16}$$

Here, $\hat{\mathbf{s}}^{(\mathrm{R})}$ and $\hat{\mathbf{s}}^{(\mathrm{R})}_\mu$ correspond, respectively, to the unit wavevector $\hat{\mathbf{s}}(\alpha^{(\mathrm{R})},\beta)$ and polarization vector $\hat{\mathbf{s}}_\mu(\alpha^{(\mathrm{R})},\beta)$ of reflected field. The angle of reflection $\alpha^{(\mathrm{R})}$ is given by $\alpha^{(\mathrm{R})}=\pi-\alpha$. Also, $\hat{\mathbf{s}}^{(\mathrm{T})}$ and $\hat{\mathbf{s}}^{(\mathrm{T})}_\mu$ are the unit wavevector $\hat{\mathbf{s}}(\alpha^{(\mathrm{T})},\beta)$ and polarization vector $\hat{\mathbf{s}}_\mu(\alpha^{(\mathrm{T})},\beta)$ of transmitted field, respectively. The angle of refraction $\alpha^{(\mathrm{T})}$ is given by $\sin\alpha=n\sin\alpha^{(\mathrm{T})}$. $\alpha^{(\mathrm{T})}$ takes the contour $C_-$, because Eq. (16) should converge for $z<0$. The reflection coefficient $\Re_\mu$ and transmission coefficient $\mathfrak{T}_\mu$ are obtained via Fresnel relations[17] as

$$\begin{aligned}\Re_\mu&=\Re_\mu(\alpha,\alpha^{(\mathrm{T})})\\ &=\frac{\cos\alpha-n\cos\alpha^{(\mathrm{T})}}{\cos\alpha+n\cos\alpha^{(\mathrm{T})}}\delta_{\mu,\mathrm{TE}}+\frac{n\cos\alpha-\cos\alpha^{(\mathrm{T})}}{n\cos\alpha+\cos\alpha^{(\mathrm{T})}}\delta_{\mu,\mathrm{TM}},\end{aligned} \tag{17}$$

$$\begin{aligned}\mathfrak{T}_\mu&=\mathfrak{T}_\mu(\alpha,\alpha^{(\mathrm{T})})\\ &=\frac{2\cos\alpha}{\cos\alpha+n\cos\alpha^{(\mathrm{T})}}\delta_{\mu,\mathrm{TE}}+\frac{2\cos\alpha}{n\cos\alpha+\cos\alpha^{(\mathrm{T})}}\delta_{\mu,\mathrm{TM}}.\end{aligned} \tag{18}$$

In addition, the electric field emitted directly by the multipole into its upper half-space $z_0>0$ (labeled by superscript D) can be derived from Eqs. (5) and (13) as

$$\mathbf{E}^{\lambda(\mathrm{D})}_{K,J,m}(\mathbf{r})=\frac{iK}{2\pi}\sum_{\mu}\int_{C_+}\int_{-\pi}^{+\pi}d\Omega_{\hat{\mathbf{s}}}f_{\lambda,J,m}(\mu,\alpha,\beta)\hat{\mathbf{s}}^{(\mathrm{D})}_{\mu}e^{iK\hat{\mathbf{s}}^{(\mathrm{D})}\cdot\mathbf{r}},$$
$$\text{for } z_{\mathrm{R}}<z$$
$$=0,\ \text{for } z<z_{\mathrm{R}} \tag{19}$$

where $\hat{\mathbf{s}}^{(\mathrm{D})}$ and $\hat{\mathbf{s}}^{(\mathrm{D})}_{\mu}$ indicate $\hat{\mathbf{s}}(\alpha,\beta)$ and $\hat{\mathbf{s}}_{\mu}(\alpha,\beta)$, respectively.

The total electric field radiated by the multipole plus surface system is obtained simply by adding field components:

$$\mathbf{E}(\mathbf{r})=\mathbf{E}^{\lambda(\mathrm{D})}_{K,J,m}(\mathbf{r})+\mathbf{E}^{\lambda(\mathrm{I})}_{K,J,m}(\mathbf{r})+\mathbf{E}^{\lambda(\mathrm{R})}_{K,J,m}(\mathbf{r})+\mathbf{E}^{\lambda(\mathrm{T})}_{K,J,m}(\mathbf{r}). \tag{20}$$

The magnetic field associated with the radiated electric field is obtained from Maxwell's equation

$$\nabla\times\mathbf{E}(\mathbf{r},t)=-(\partial/\partial t)\mathbf{B}(\mathbf{r},t)=iK\mathbf{B}(\mathbf{r},t), \tag{21}$$

with the relation between unit wavevector and polarization vector

$$\hat{\mathbf{s}}^{(\sigma)}\times\hat{\mathbf{s}}^{(\sigma)}_{\mu}=\eta_{\mu}\hat{\mathbf{s}}^{(\sigma)}_{\mu}\ \text{for}\ \sigma=\mathrm{I,R,T,D}. \tag{22}$$

The results are given by

$$\mathbf{B}^{\lambda(\mathrm{I})}_{K,J,m}(\mathbf{r})=\frac{iK}{2\pi}\sum_{\mu}\eta_{\mu}\int_{C_-}\int_{-\pi}^{+\pi}d\Omega_{\hat{\mathbf{s}}}f_{\lambda,J,m}(\mu,\alpha,\beta)\hat{\mathbf{s}}^{(\mathrm{I})}_{\mu}e^{iK\hat{\mathbf{s}}^{(\mathrm{I})}\cdot\mathbf{r}},$$
$$\text{for } 0\le z<z_R$$
$$=0,\ \text{for } z<0,\ z_R<z \tag{23}$$

$$\mathbf{B}^{\lambda(\mathrm{R})}_{K,J,m}(\mathbf{r})=\frac{iK}{2\pi}\sum_{\mu}\eta_{\mu}\int_{C_-}\int_{-\pi}^{+\pi}d\Omega_{\hat{\mathbf{s}}}f_{\lambda,J,m}(\mu,\alpha,\beta)\Re_{\mu}\hat{\mathbf{s}}^{(\mathrm{R})}_{\mu}e^{iK\hat{\mathbf{s}}^{(\mathrm{R})}\cdot\mathbf{r}},$$
$$\text{for } z\ge 0$$
$$=0,\ \text{for } 0<z \tag{24}$$

$$\mathbf{B}^{\lambda(\mathrm{T})}_{K,J,m}(\mathbf{r})=\frac{iK}{2\pi}\sum_{\mu}\eta_{\mu}\int_{C_-}\int_{-\pi}^{+\pi}d\Omega_{\hat{\mathbf{s}}}f_{\lambda,J,m}(\mu,\alpha,\beta)n\mathfrak{T}_{\mu}\hat{\mathbf{s}}^{(\mathrm{T})}_{\mu}e^{inK\hat{\mathbf{s}}^{(\mathrm{T})}\cdot\mathbf{r}},$$
$$\text{for } z<0$$
$$=0,\ \text{for } z\ge 0 \tag{25}$$

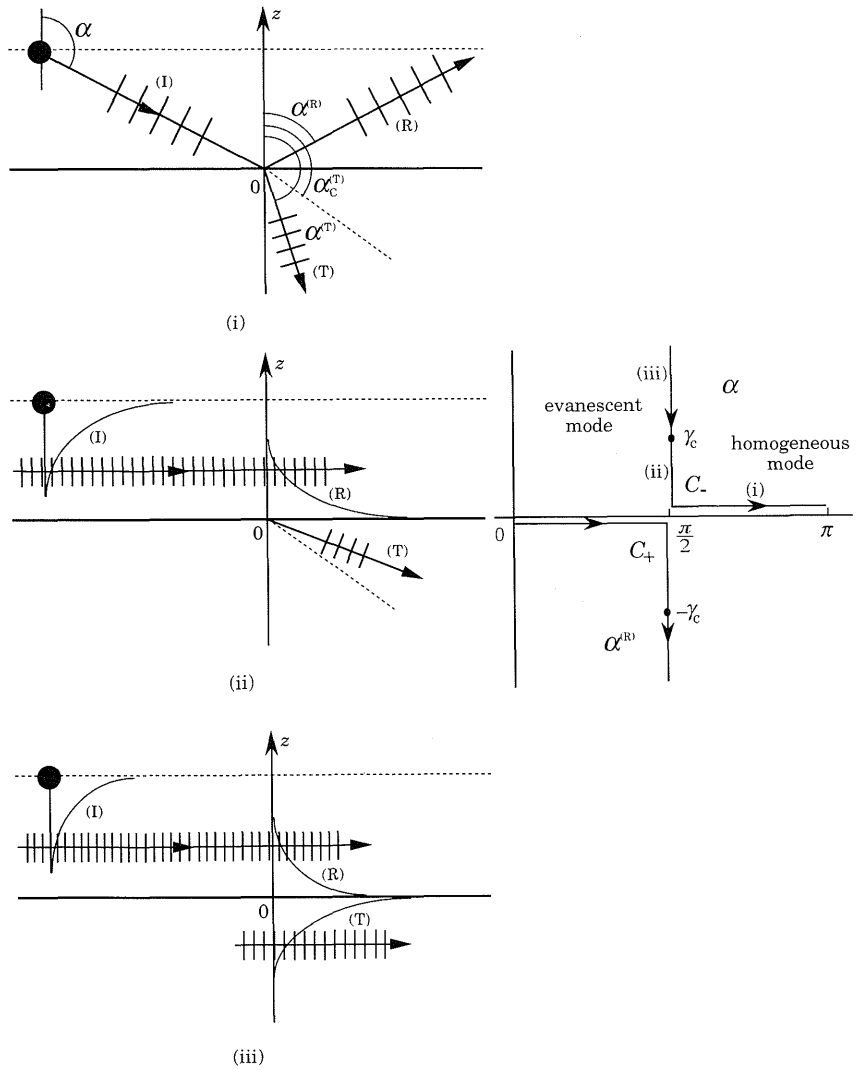


Fig. 5. Three characteristic scattering processes of multipole field described in terms of angular spectrum representation. (i) When the incident and reflected fields are homogeneous, $(\pi/2)<\alpha\le\pi$, the transmitted field is homogeneous, $\alpha_c^{(\mathrm{T})}<\alpha^{(\mathrm{T})}\le\pi$. (ii) When the incident and reflected fields are evanescent, $\alpha=(\pi/2)+i\gamma$, $0\le\gamma<\gamma_c$, the transmitted field is homogeneous, $\alpha_c^{(\mathrm{T})}\ge\alpha^{(\mathrm{T})}>(\pi/2)$. (iii) When the incident field is evanescent, $\alpha=(\pi/2)+i\gamma$, $\gamma_c\le\gamma<\infty$, the reflected field is evanescent, $\alpha^{(\mathrm{R})}=(\pi/2)-i\gamma$, $\gamma_c\le\gamma<\infty$, and the transmitted field is evanescent, $\alpha=(\pi/2)+i\gamma^{(\mathrm{T})}$, $0\le\gamma^{(\mathrm{T})}<\infty$.

$$\mathbf{B}^{\lambda(\mathrm{D})}_{K,J,m}(\mathbf{r})=\frac{iK}{2\pi}\sum_{\mu}\eta_{\mu}\int_{C_+}\int_{-\pi}^{+\pi}d\Omega_{\hat{\mathbf{s}}}f_{\lambda,J,m}(\mu,\alpha,\beta)\hat{\mathbf{s}}^{(\mathrm{D})}_{\mu}e^{iK\hat{\mathbf{s}}^{(\mathrm{D})}_{\mu}\cdot\mathbf{r}},$$
$$\text{for } z_{\mathrm{R}}<z$$
$$=0,\ \text{for } z<z_{\mathrm{R}} \tag{26}$$

The total magnetic field radiated by the multipole plus surface system is obtained by adding these field components:

$$\mathbf{B}(\mathbf{r})=\mathbf{B}^{\lambda(\mathrm{D})}_{K,J,m}(\mathbf{r})+\mathbf{B}^{\lambda(\mathrm{I})}_{K,J,m}(\mathbf{r})+\mathbf{B}^{\lambda(\mathrm{R})}_{K,J,m}(\mathbf{r})+\mathbf{B}^{\lambda(\mathrm{T})}_{K,J,m}(\mathbf{r}). \tag{27}$$

Investigating the angular spectrum representation derived for the incident, reflected and transmitted fields, we find that the scattered multipole field by the planar dielectric surface involves the following three characteristic processes (see Fig. 5).

(i) When the incident and reflected fields are homogeneous, $(\pi/2)<\alpha\leq\pi$, the transmitted field is homogeneous, $\alpha_{\mathrm{c}}^{(\mathrm{T})}<\alpha^{(\mathrm{T})}\leq\pi$, where $\alpha_{\mathrm{c}}^{(\mathrm{T})}$ is the critical angle defined by $\sin\alpha_{\mathrm{c}}^{(\mathrm{T})}=(1/n)$.

(ii) When the incident and reflected fields are evanescent, i.e. $\alpha=(\pi/2)+i\gamma$, $0\leq\gamma<\gamma_{\mathrm{c}}$, with the critical angle $(\pi/2+i\gamma_{\mathrm{c}})$ related by $\sin(\pi/2+i\gamma_{\mathrm{c}})=n$, the transmitted field is homogeneous, $\alpha_{\mathrm{c}}^{(\mathrm{T})}\geq\alpha^{(\mathrm{T})}>(\pi/2)$.

(iii) When the incident field is evanescent, $\alpha=(\pi/2)+i\gamma$, $\gamma_{\mathrm{c}}\leq\gamma<\infty$, the reflected field is evanescent, $\alpha^{(\mathrm{R})}=(\pi/2)-i\gamma$, $\gamma_{\mathrm{c}}\leq\gamma<\infty$, and the transmitted field is totally evanescent, i.e., $\alpha=(\pi/2)+i\gamma^{(\mathrm{T})}$, $0\leq\gamma^{(\mathrm{T})}<\infty$.

Case (iii) is particularly interesting because this involves surface electromagnetic modes with wavevectors parallel to the surface, which is larger than that of the propagating mode both in dielectric and vacuum. This is the origin of the lateral spatial locality of the multipole-surface interaction in the near-field regime. Case (iii) thus corresponds to the multiple scattering process taking place between the multipole and the electromagnetic mode localized on the dielectric surface which can be observed in the far field only via multiple scattering process.

## 4. The Far-Field Behavior of the Radiated Fields

In the usual far field observation regime of radiation properties of the excited atoms or molecules near a dielectric surface ($Kz_{\mathrm{R}}\ll1$), the light detector is placed at a point in the upper or lower hemisphere with the radius $r$ satisfying the far-field condition $Kr\gg1$ or $nKr\gg1$. In this section, let $\mathfrak{A}_1$ and $\mathfrak{A}_2$ be these upper and lower hemispheres for observation (Fig. 6). To compare our results with far-field observations, let us investigate the asymptotic behaviors of our fomulae. Of course, if we employ a near-field measurement scheme by using a sharpened optical fiber probe, we can observe the field distribution with subwavelength resolution. However, in such near-field measurements a detailed evaluation of the interaction between the probe-tip with the multipole plus surface system should be considered, which includes multiple scattering processes. This will be discussed using our formulations elsewhere.

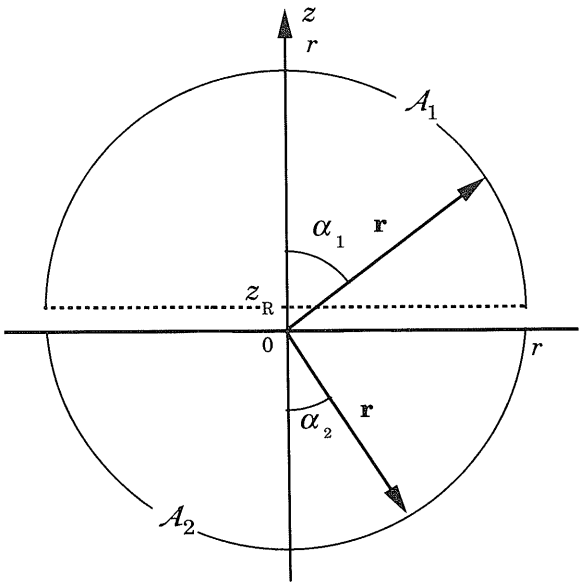


Fig. 6. Upper and lower hemisphere, $\mathfrak{A}_1$ and $\mathfrak{A}_2$ for observation. Their radii $r$ are considered to satisfy the far field observation conditions $Kr\gg1$ and $nKr\gg1$ at upper and lower spaces, respectively.

### *4.1 Asymptotic Forms of the Scattered Fields on $\mathfrak{A}_1$ (Vacuum Side)*

In the upper half-space of the multipole, $z_{\mathrm{R}}<z$, (see Fig. 4), the electric and magnetic fields are written, respectively, by

$$\mathbf{E}^{\lambda}_{K,J,m}(\mathbf{r})=\mathbf{E}^{\lambda(\mathrm{D})}_{K,J,m}(\mathbf{r})+\mathbf{E}^{\lambda(\mathrm{R})}_{K,J,m}(\mathbf{r}). \tag{28}$$

$$\mathbf{B}^{\lambda}_{K,J,m}(\mathbf{r})=\mathbf{B}^{\lambda(\mathrm{D})}_{K,J,m}(\mathbf{r})+\mathbf{B}^{\lambda(\mathrm{R})}_{K,J,m}(\mathbf{r}). \tag{29}$$

First, we consider the asymptotic forms of Eqs. (19) and (26) at a position on the observation hemisphere $\mathfrak{A}_1$ in the far field specified by the directional unit vector $\hat{\mathbf{r}}=\mathbf{r}/r$ and (real) spherical polar angles $(\alpha_1,\beta_1)$, $(0\leq\alpha_1<\pi/2$ on the contour $C_+)$. The asymptotic forms can be obtained by replacing Eqs. (19) and (26) by their angular spectrum representations in the form of Eq. (9) and by applying stationary phase method for double integrals involved in these representations.[14].

In the far-field region, only the plane wave with unit (real) wavevector $\hat{\mathbf{s}}=\hat{\mathbf{r}}$ (i.e., $\alpha=\alpha_1$, $\beta=\beta_1$) makes a significant contribution to the integral. Therefore, the results are given by

$$\mathbf{E}^{\lambda(\mathrm{D})}_{K,J,m}(\mathbf{r})\sim\sum_{\mu}f^{(\mathrm{D})}_{\lambda,J,m}(\mu,\alpha_1,\beta_1)\hat{\mathbf{s}}_{1,\mu}\frac{e^{iKr}}{r}, \tag{30}$$

$$\mathbf{B}^{\lambda(\mathrm{D})}_{K,J,m}(\mathbf{r})\sim\sum_{\mu}\eta_{\mu}f^{(\mathrm{D})}_{\lambda,J,m}(\mu,\alpha_1,\beta_1)\hat{\mathbf{s}}_{1,\bar{\mu}}\frac{e^{iKr}}{r}, \tag{31}$$

where the polarization vector $\hat{\mathbf{s}}_{1,\mu}$, indicates $\hat{\mathbf{s}}_{\mu}(\alpha_1,\beta_1)$, and the scattered amplitude is given by

$$f^{(\mathrm{D})}_{\lambda,J,m}(\mu,\alpha_1,\beta_1)=f_{\lambda,J,m}(\mu,\alpha_1,\beta_1). \tag{32}$$

Next, we consider the asymptotic forms of Eqs. (15) and (24) at a position on $\mathfrak{A}_1$, with direction specified by unit vector $\hat{\mathbf{r}}$. In this case, the only significant contribution is

from the reflected plane wave with unit (real) wavevector $\hat{\mathbf{s}}^{(\mathrm{R})}=\hat{\mathbf{r}}$ (i.e. $\alpha=\pi-\alpha_1$, $\beta=\beta_1$). Then, the asymptotic forms are given by

$$\mathbf{E}^{\lambda(\mathrm{R})}_{K,J,m}(\mathbf{r})\sim\sum_{\mu}f^{(\mathrm{R})}_{\lambda,J,m}(\mu,\pi-\alpha_1,\beta_1)\hat{\mathbf{s}}_{1,\mu}\frac{e^{iKr}}{r}, \tag{33}$$

$$\mathbf{B}^{\lambda(\mathrm{R})}_{K,J,m}(\mathbf{r})\sim\sum_{\mu}\eta_{\mu}f^{(\mathrm{R})}_{\lambda,J,m}(\mu,\pi-\alpha_1,\beta_1)\hat{\mathbf{s}}_{1,\bar{\mu}}\frac{e^{iKr}}{r}, \tag{34}$$

where the scattered amplitude is given by

$$f^{(\mathrm{R})}_{\lambda,J,m}(\mu,\pi-\alpha_1,\beta_1)=f_{\lambda,J,m}(\mu,\pi-\alpha_1,\beta_1)\Re_{\mu}(\pi-\alpha_1,\pi-\alpha_2). \tag{35}$$

The angle $\alpha_2$ is related to $\alpha_1$ as $\sin\alpha_1=n\sin\alpha_2$ and takes the contour $C_+$. Because the reflected angle $\alpha_1$ takes $0\leq\alpha_1<(\pi/2)$, $\alpha_2$ is a real number lying in the region $0\leq\alpha_2<\alpha_{2,\mathrm{c}}=\arcsin(1/n)$.

From Eqs. (28) and (29), the asymptotic forms of the electric and magnetic fields on $\mathfrak{A}_1$ are given, respectively, by

$$\mathbf{E}^{\lambda}_{K,J,m}(\mathbf{r})\sim\sum_{\mu}[f^{(\mathrm{D})}_{\lambda,J,m}(\mu,\alpha_1,\beta_1)+f^{(\mathrm{R})}_{\lambda,J,m}(\mu,\pi-\alpha_1,\beta_1)]\hat{\mathbf{s}}_{1,\mu}\frac{e^{iKr}}{r}, \tag{36}$$

$$\mathbf{B}^{\lambda}_{K,J,m}(\mathbf{r})\sim\sum_{\mu}\eta_{\mu}[f^{(\mathrm{D})}_{\lambda,J,m}(\mu,\alpha_1,\beta_1)+f^{(\mathrm{R})}_{\lambda,J,m}(\mu,\pi-\alpha_1,\beta_1)]\hat{\mathbf{s}}_{1,\bar{\mu}}\frac{e^{iKr}}{r}. \tag{37}$$

*4.2 Asymptotic Forms of the Fields on $\mathfrak{A}_2$ (Dielectric Side)*

In the dielectric region $z<0$ (see Fig. 4), the electric and magnetic fields are written, respectively, by

$$\mathbf{E}^{\lambda}_{K,J,m}(\mathbf{r})=\mathbf{E}^{\lambda(\mathrm{T})}_{K,J,m}(\mathbf{r}), \tag{38}$$

$$\mathbf{B}^{\lambda}_{K,J,m}(\mathbf{r})=\mathbf{B}^{\lambda(\mathrm{T})}_{K,J,m}(\mathbf{r}), \tag{39}$$

Let us consider the asymptotic form of the transmitted fields, Eqs. (16) and (25), at a position on $\mathfrak{A}_2$ with direction specified by unit vector $\hat{\mathbf{r}}=\mathbf{r}/r$ and (real) spherical polar angles $(\pi-\alpha_2,\beta_2)$ $(0\leq\alpha_2<(\pi/2)$ taking the contour $C_+$). When we consider the asymptotic form on $\mathfrak{A}_2$ using angular spectrum representation of the form of Eq. (9) for Eqs. (16) and (25), only the plane wave with unit (real) wavevector $\hat{\mathbf{s}}^{(\mathrm{T})}=\hat{\mathbf{r}}$ (i.e., $\alpha^{(\mathrm{T})}=\pi-\alpha_2$, $\beta=\beta_2$) contributes significantly. Let the angle $\alpha_1$ defined by $\sin\alpha_1=n\sin\alpha_2$ which takes the contour $C_+$. The asymptotic forms are obtained as

$$\mathbf{E}^{\lambda}_{K,J,m}(\mathbf{r})\sim n\sum_{\mu}f^{(\mathrm{T})}_{\lambda,J,m}(\mu,\pi-\alpha_1,\beta_1)\hat{\mathbf{s}}_{2,\mu}\frac{e^{inKr}}{r}, \tag{40}$$

$$\mathbf{B}^{\lambda}_{K,J,m}(\mathbf{r})\sim n^2\sum_{\mu}\eta_{\mu}f^{(\mathrm{T})}_{\lambda,J,m}(\mu,\pi-\alpha_1,\beta_1)\hat{\mathbf{s}}_{2,\bar{\mu}}\frac{e^{inKr}}{r}, \tag{41}$$

where the scattered amplitude is given by

$$f^{(\mathrm{T})}_{\lambda,J,m}(\mu,\pi-\alpha_1,\beta_1)=f_{\lambda,J,m}(\mu,\pi-\alpha_1,\beta_1)\frac{\cos(\pi-\alpha_2)}{\cos(\pi-\alpha_1)}\mathfrak{T}_{\mu}(\pi-\alpha_1,\pi-\alpha_2), \tag{42}$$

and $\hat{\mathbf{s}}_{2,\mu}$ is the polarization vector of transmitted wave with the spherical polar angles $(\pi-\alpha_2,\beta_2)$, and $\beta_1=\beta_2$.

## 5. The Angular Distribution of Light Emission from Multipole

The energy flux through the infinitesimal area $r^2\sin\alpha_1 d\alpha_1 d\beta_1$ on $\mathfrak{A}_1$, and also that through $r^2\sin\alpha_2 d\alpha_2 d\beta_2$ on $\mathfrak{A}_2$, are given by

$$d\mathrm{I}^{\lambda}_{K,J,m}(\alpha_i,\beta_i)=\mathbf{P}^{\lambda}_{K,J,m}(\mathbf{r})\cdot\hat{\mathbf{s}}_i r^2 d\Omega_i,\ i=1,2. \tag{43}$$

Here, $\mathbf{P}^{\lambda}_{K,J,m}(\mathbf{r})$ indicates Poynting vector given by

$$\mathbf{P}^{\lambda}_{K,J,m}(\mathbf{r})=\mathbf{E}^{\lambda}_{K,J,m}(\mathbf{r})\times[\mathbf{B}^{\lambda}_{K,J,m}(\mathbf{r})]^*. \tag{44}$$

The unit vectors $\hat{\mathbf{s}}_1$ and $\hat{\mathbf{s}}_2$ correspond, respectively, to $\hat{\mathbf{s}}(\alpha_1,\beta_1)$ and $\hat{\mathbf{s}}(\pi-\alpha_2,\beta_2)$, and the solid angle $d\Omega_i=\sin\alpha_i d\alpha_i d\beta_i$. Substituting the asymptotic forms of the fields into Eq. (44) and using the relation between the (real) polarization vectors

$$\hat{\mathbf{s}}_{\nu,\mu}\times[\eta_{\mu'}\hat{\mathbf{s}}_{\nu,\bar{\mu}'}]^*=\eta_{\mu'}\hat{\mathbf{s}}_{\nu,\mu}\times\hat{\mathbf{s}}_{\nu,\bar{\mu}'}=\delta_{\mu,\mu'}\hat{\mathbf{s}}_{\nu},\ \text{for}\ \nu=1,2, \tag{45}$$

we can obtain the angular distribution of the radiation field on the observation hemispheres $\mathfrak{A}_1$ and $\mathfrak{A}_2$ written as the sum of the angular distributions of TE and TM polarized light:

$$\frac{d\mathrm{I}^{\lambda}_{K,J,m}(\alpha_i,\beta_i)}{d\Omega_i}=\sum_{\mu}\frac{d\mathrm{I}^{\lambda}_{K,J,m}(\alpha_i,\beta_i;\mu)}{d\Omega_i},\ \text{on}\ \mathfrak{A}_i,\ i=1,2. \tag{46}$$

The angular distributions of $\mu$-polarized light on $\mathfrak{A}_i$ are given by

$$\frac{d\Omega^{\lambda}_{K,J,m}(\alpha_1,\beta_1;\mu)}{d\Omega_1}=|g_{\lambda,J,m}(\mu,\alpha_1,\beta_1)+g_{\lambda,J,m}(\mu,\pi-\alpha_1,\beta_1)\Re_{\mu}(\pi-\alpha_1,\pi-\alpha_2)|^2, \tag{47}$$

$$\frac{d\mathrm{I}^{\lambda}_{K,J,m}(\alpha_2,\beta_2;\mu)}{d\Omega_2}=n^3\left|g_{\lambda,J,m}(\mu,\pi-\alpha_1,\beta_1)\frac{\cos(\pi-\alpha_2)}{\cos(\pi-\alpha_1)}\mathfrak{T}_{\mu}(\pi-\alpha_1,\pi-\alpha_2)\right|^2. \tag{48}$$

Here, the function $g_{\lambda,J,m}$ is given by

$$g_{\lambda,J,m}(\mu,\alpha,\beta)=(\mu,\alpha,\beta|\lambda,J,m)e^{-i\rho\cos\alpha}, \tag{49}$$

with normalized multipole-surface distance, $\rho=Kz_{\mathrm{R}}$.

## 6. Numerical Evaluation of the Angular Distribution of Light Emission from the Electric Dipole Near Planar Dielectric Surface

As an example, we evaluate the angular distribution of light emission from the electric dipole ($\lambda=E$, $J=1$) with magnitude $d$ and arbitrary orientation $(\Theta,\Phi)$, which is located at position $\mathbf{R}$ as shown in Fig. 1. The electric dipole can be described by

$$\mathbf{d}=\sum_{m=-1}^{+1}(-1)^m d_{-m}\hat{\mathbf{e}}_m, \tag{50}$$

with the base polarizations defined by

$$d_{+1}=-\frac{1}{\sqrt{2}}(d_x+id_y)=-\frac{1}{\sqrt{2}}d\sin\Theta e^{+i\Phi}$$
$$d_0=d_z=d\cos\Theta,$$
$$d_{-1}=+\frac{1}{\sqrt{2}}(d_x-id_y)=+\frac{1}{\sqrt{2}}d\sin\Theta e^{-i\Phi}. \tag{51}$$

In this representation, the vector potential for radiation field is given as a superposition of Eq. (5) with different numbers of $m$:

$$\mathbf{A}^{\mathrm{E(RA)}}_{K,1}(\mathbf{r}_0)=\sum_{m=-1}^{+1}(-1)^m d_{-m}\mathbf{A}^{\mathrm{E(RA)}}_{K,J,m}(\mathbf{r}_0)\,. \tag{52}$$

Thus the angular distribution of the $\mu$(TE,TM)-polarized light on $\mathfrak{A}_2$ is given by

$$\frac{dI^E_{K,1}(\alpha_2,\beta_2;\mu)}{d\Omega_2}=n^3\left|\sum_m(-1)^m d_{-m}g_{E,1,m}(\mu,\pi-\alpha_1,\beta_1)\times\frac{\cos(\pi-\alpha_2)}{\cos(\pi-\alpha_1)}\mathfrak{T}_\mu(\pi-\alpha_1,\pi-\alpha_2)\right|^2. \tag{53}$$

From Eqs. (6)-(8), the expansion coefficients are given by

$$(\mathrm{TE},\pi-\alpha_1,\beta_1|\mathrm{E},1,m)=-\frac{i}{4}\sqrt{\frac{3}{\pi}}[e^{+i\beta_1}\delta_{m,+1}+e^{-i\beta_1}\delta_{m,-1}]\,, \tag{54}$$

$$(\mathrm{TM},\pi-\alpha_1,\beta_1|\mathrm{E},1,m)=-\frac{1}{4}\sqrt{\frac{3}{\pi}}[-\cos\alpha_1 e^{+i\beta_1}\delta_{m,+1}+\sqrt{2}\sin\alpha_1\delta_{m,0}+\cos\alpha_1 e^{-i\beta_1}\delta_{m,-1}]\,. \tag{55}$$

The results are given by

$$\frac{dI^E_{K,1}(\alpha_2,\beta_2;\mathrm{TE})}{d\Omega_2}=\frac{3n^3d^2}{2\pi}\left|\frac{\cos\alpha_2\sin\Theta\sin(\beta_1-\Phi)}{\cos\alpha_1+n\cos\alpha_2}e^{i\rho\cos\alpha_1}\right|^2,$$

$$\frac{dI^E_{K,1}(\alpha_2,\beta_2;\mathrm{TM})}{d\Omega_2}=\frac{3n^3d^2}{2\pi}\left|\frac{\cos\alpha_2(\cos\Theta\sin\alpha_1+\sin\Theta\cos(\beta_1-\Phi)\cos\alpha_1)}{n\cos\alpha_1+\cos\alpha_2}e^{i\rho\cos\alpha_1}\right|^2, \tag{56}$$

Our results for the electric dipole case are in agreement with those of Lukosz[9] at $\Phi=0$ and provide more generalized ones.

When $0\le\alpha_2<\alpha_{2c}$, $\sin\alpha_{2c}=1/n$, $\alpha_1$ is real ($0\le\alpha_1<\pi/2$), so that the field emitted by the electric dipole is homogeneous. Since $|e^{i\rho\cos\alpha_1}|=1$, the angular distribution is independent of the distance $z_R$ from the surface.

When $\alpha_{2c}\le\alpha_2<\pi/2$, $\alpha_1$ is complex ($\alpha_1=\pi/2-i\gamma_1(0\le\gamma_1<\gamma_{1c})$), where $\sin(\pi/2-i\gamma_{1c})=n$, the angular distribution is dependent on $z_R$ since $|e^{i\rho\cos\alpha}|=e^{-\rho\sinh\gamma_1}$. An evanescent wave emitted by the electric dipole is transmitted into $\alpha_{2c}\le\alpha_2<\pi/2$ (see Fig. 5).

Figure 7 shows our theoretical results for $n=\sqrt{2}$ ($\alpha_{2c}=\pi/2$), $\rho=1$, and $\beta_1=0$ ($xz$ plane). In this situation, the angular distribution of light emission from electric dipole $\mathbf{d}_x$ and $\mathbf{d}_z$ involve only TM polarized modes in far field. Also, that for electric dipole $\mathbf{d}_y$ is determined only by that which corresponds to the TE polarization, because the transmitted dipole field is TE polarized in far field. The comparison of these theoretical results with experimental results was reported previously.[4] In the experiments in Ref. 4) the optical transition occurred between hyperfine states of Cs atom, so that the polarization states, $\mathbf{d}_x$, $\mathbf{d}_y$, $\mathbf{d}_z$ were mixed due to hyperfine coupling even for the TE/TM polarized excited light. The result was averaged over the distance $z_R$ from the surface, since the experiments were done for Cs vapor. The theoretical calculation reproduced the experimental results very well.

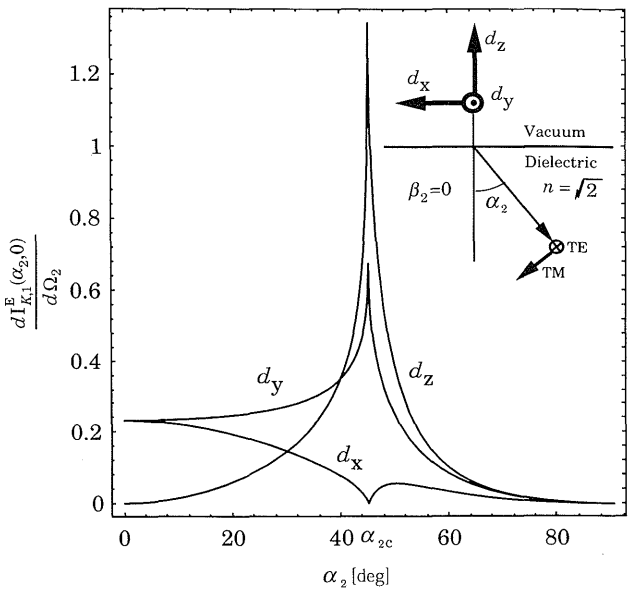


Fig. 7. The calculated results of angular distribution of light emission from electric dipoles with polarization vectors $\mathbf{d}_x$, $\mathbf{d}_y$ and $\mathbf{d}_z$. The light emission is observed at the intersection of the hemisphere $\mathfrak{A}_2$ and $xz$ plane.

## 7. Conclusions

We have derived the general analytic expressions for angular distribution of light emission from electric and magnetic multipoles near a dielectric surface, using the angular spectrum representation of vector spherical waves. The results are described in terms of spatial rotation matrix elements, so that the angular distribution of light emission for high order multipoles is easily obtained. The numerical results for electric dipole are in good agreement with our previous experiments. From the angular spectrum representation of multipole fields, we analyzed the three characteristic properties of the multipole-surface interaction. One of these processes involves the surface-electromagnetic modes, which is the origin of the lateral spatial locality of the multipole-surface interaction in the near-field regime. The formulation developed in this paper is directly applicable to near-field measurements of scattered multipole field using a sharpened optical fiber probe. A detailed evaluation of the interaction between the probe-tip with the multipole near a dielectric surface will be discussed elsewhere using our formulations.

### Acknowledgments

The authors would like to express their thanks to Profs. W. Jhe, K. Kitahara, and I. Banno for useful discussions and comments, and to Dr. T. Matsudo and Prof. T. Sakurai for collaboration and useful discussions. This work was supported by a Grant-in-Aid for Scientific Research from the Ministry of Education, Science, Sports and Culture of Japan.

## References


1) See, for example, articles in *Near Field Optics*, eds. D.W. Pohl and D. Courjon (Kluwer Academic Publishers, Netherlands, 1993).
2) J.M. Wylie and J.E. Sipe: Phys. Rev. A **30** (1984) 1185.
3) G.S. Agarwal: Phys. Rev. A **11** (1975) 230.
4) T. Matsudo, T. Inoue, Y. Inoue, H. Hori and T. Sakurai: Phys. Rev. A **55** (1997) 2406.
5) C.K. Carniglia, L. Mandel and K.H. Drexhage: J. Opt. Soc. Am. **62** (1972) 479.
6) A.L. Burgmans and M.F. Schuurmans: Phys. Rev. A **16** (1977) 2002.
7) W. Lukosz and R.E. Kunz: J. Opt. Soc. Am. **67** (1977) 1607.
8) W. Lukosz and R.E. Kunz: J. Opt. Soc. Am. **67** (1977) 1615.
9) W. Lukosz: J. Opt. Soc. Am. **69** (1979) 1495.
10) T. Inoue and H. Hori: Opt. Rev. **3** (1996) 458.
11) A.S. Davydov: *Quantum Mechanics* (Pergamon Press, Oxford, 1965) 1st ed. Chap. XIV, Sect. 135, p. 578.
12) A.R. Edmonds: *Angular Momentum in Quantum Mechanics* (Princeton University Press, Princeton, 1974) 2nd ed., Chap. 5, Sect. 5.9, p. 81.
13) E. Wolf and M. Nieto-Vesperinas: J. Opt. Soc. Am. A **2** (1985) 886.
14) M. Born and E. Wolf: *Principles of Optics* (Pergamon Press, Oxford 1975) 6th ed., Appendix. III, Sect. 3, p. 753.
15) R. Asby and E. Wolf: J. Opt. Soc. Am. **61** (1971) 52.
16) K. Miyamoto and E. Wolf: J. Opt. Soc. Am. **52** (1962) 615.
17) C.K. Carniglia and L. Mandel: Phys. Rev. D **3** (1971) 280.